SCANS: Efficient Densest Subgraph Discovery over Relational Graphs without Materialization

Anonymous Author(s)

ABSTRACT

Driven by applications such as fraud detection and protein complex discovery, there has been extensive work on developing exact or approximation algorithms for efficient densest subgraph discovery in graphs of financial transactions and protein-protein interactions respectively. At the core of these applications is the application data in the form of relations from which the corresponding graphs, called relational graphs, are derived which are then used to find the densest subgraphs. Most existing approaches assume that these relational graphs are already derived and materialized and focus on efficient discovery of the densest subgraph. Unfortunately, materializing these graphs can be resource-intensive, which thus limits the practical usefulness of existing algorithms over large datasets. To mitigate this, we propose a novel SketCh-bAsed deNsest Subgraph discovery (SCANS) system. A notable feature of SCANS is that it offers user-defined APIs for customizing peeling algorithms, a popular class of algorithms for densest subgraph discovery, for different density metrics, without the need for graph materialization. Our unique *sketch-based peeling* algorithm forms the core of SCANS. Following the peeling paradigm, it utilizes sketches to efficiently estimate peeling coefficients and subgraph densities at each peeling iteration and thus avoids materializing the relational graph completely. Through extensive experiments, we demonstrate the efficacy and efficiency of SCANS, reaching orders of magnitude speedups compared to the conventional baselines with materialization, while consistently achieving at least 95% accuracy compared to peeling algorithms based on materialization.

1 INTRODUCTION

Discovering dense subgraphs in a given network has broad applications in different domains such as system optimization by social piggybacking [16], discovery of protein complexes [34, 42], information dissemination analysis to discover filter bubbles and echo chambers [26, 27, 29], and forms a building block of many graph problems including reachability queries [12]. Most prior studies on densest subgraph discovery assume that a materialized data graph is available and accessible with low latency. However, in many applications, the underlying network on which to discover densest subgraphs is not explicitly available and tends to be present implicitly in the form of complex relationships between entities in the application. These relational graphs [41] need to be carefully extracted from heterogeneous data sources such as knowledge graphs (KGs) [19, 21] and relational databases [2, 36] and the extraction is time-consuming. For example, it takes more than 1200 seconds to materialize the co-purchase graph from the TPCH benchmark [43] (which is a relational database) with join operations.

In this study, we follow the *meta-path* semantics [13, 30, 37, 44] — a prevalent method for deriving relational graphs from diverse data sources. Our core objective is to address the challenge of *densest subgraph discovery* (DSD) within relational graphs shaped by a specific meta-path $\mathcal{M}$, while avoiding the need to materialize them.

Applications. The discovery of densest subgraphs in relational graphs is pivotal in numerous real-world contexts, including:

- *Fraud Detection.* In e-commerce platforms, fraud, such as promotion abuse, is common where fraudsters exploit promotions by creating fake accounts to unfairly benefit from offers. They often log into various accounts using a limited number of devices. This relationship between accounts and devices can be represented by meta-paths "(user)→(*account*) → (*device*)". DSD in this context serves as a strong indicator of potential fraudulent activities, aiding in the detection and prevention of such schemes [9, 22].
- *Identifying Filter Bubbles.* Filter bubbles and echo chambers occur in social networks, creating environments where users are exposed primarily to ideas and viewpoints similar to their own, thus limiting content diversity and exposure [26, 27, 29]. These networks, structured through meta-paths "(*user*) → (*topic*)", enable the mapping of user-topic interactions in question-answering platforms such as *Quora*. DSD within these mappings is crucial, as it highlights the concentration of similar viewpoints, signifying the possible existence of filter bubbles. This is an essential step in addressing information diversity challenges and mitigating echo chamber effects in social networks.
- *Protein Complex Discovery.* Protein-protein interaction (PPI) networks offer a detailed map of the intricate interactions among proteins that are fundamental to physiological processes. These networks are adeptly characterized through meta-paths of the form "(*protein*) → (*function*)", which articulate the functional pathways connecting proteins. Densest subgraphs within PPI networks have been found to correspond to protein complexes [34, 42]. Such complexes are not only vital for understanding the specific roles and mechanisms of proteins in cellular activities but also for unveiling potential targets for therapeutic intervention.

Challenges. Most approaches for the DSD problem assume that the underlying relational graph is extracted and materialized. *However, our experiments reveal that relational graph construction accounts for up to 99.58% of the total time needed for DSD over relational graphs.* This complexity is caused by the need for complex operations such as multiple joins in RDBMS or traversing meta-path instances in KGs. Second, the vast diversity of meta-paths in heterogeneous data sources further complicates this approach. Considering the potentially thousands of meta-paths, materializing a relational graph for each meta-path can become prohibitively expensive.

Our Contributions. To address these challenges, we propose a novel system, SketCh-bAsed deNsest Subgraph discovery (SCANS) for DSD. Our system distinguishes itself from prior studies by introducing the following novel optimizations.

Sketch-Peeling Algorithm. Sketching, an efficient technique primarily recognized for estimating distinct value counts [6], is repurposed in SCANS to serve a novel role in relational graph analysis for DSD.

This use of sketching remains largely unexplored in existing studies. Specifically, by integrating sketching with the peeling algorithm, SCANS *directly estimates* peeling coefficients and densities from heterogeneous data sources. This strategic approach sidesteps the extensive resource demands typically associated with the materialization of relational graphs. Our system showcases superior time and space efficiency over contemporary methods for detecting the densest subgraph which rely on materialized relational graphs.

Lazy Sketch Maintenance. SCANS leverages the well-known KMV sketches [5] and introduces a *lazy sketch maintenance* strategy to update KMV sketches efficiently during the DSD process. Rather than reconstructing KMV sketches at each iteration—a highly time-consuming task—we opt for a selective update mechanism. This approach maintains the sketches' relevance by adjusting them as nodes are removed, with occasional reconstructions based on a set threshold to control the balance between efficiency and the accuracy of density estimations.

Summary. We make the following contributions.

- We propose SCANS, a novel system that allows data engineers to deploy user-defined, efficient and scalable peeling algorithms for DSD over relational graphs (virtually) extracted from large heterogeneous data sources (Sec. 3.1).
- We devise a *sketch-based peeling* algorithm, which efficiently constructs and maintains the sketches for peeling coefficients and subgraph density estimation across peeling iterations (Sec. 3.2).
- We deploy our SCANS system for DSD based on edge-density and theoretically establish that SCANS can achieve $(2+\epsilon)$-approximation efficiently. For triangle-density metric, we devise novel unbiased estimators for the corresponding peeling coefficients and triangle-density based on the sketches (Sec. 4).
- Extensive experiments on real-world datasets and the TPCH benchmark demonstrate that the SCANS system scales well to large relational graphs where baselines fail to terminate in a reasonable time and achieves orders of magnitude speedup in most cases over baselines, while yielding subgraphs with at least 95% density and comparable size to the subgraph returned by peeling algorithms based on materialization (Sec. 5).

2 PRELIMINARIES

In this section, we introduce the basic notations, formulate the problem of densest subgraph discovery (DSD) over relational graphs, review the peeling paradigm for DSD and discuss the related works.

2.1 Notations and Problem Formulation

For concreteness of exposition, we model a heterogeneous data source as a knowledge graph (KG). Specifically, a KG is denoted as $\mathcal{G} = (\mathcal{V}, \mathcal{E}, \mathcal{L})$, where $\mathcal{V}$ and $\mathcal{E}$ represent the sets of nodes and edges. An edge $e \in \mathcal{E}$ connects two nodes $u, v \in \mathcal{V}$. The function $\mathcal{L}$ maps each node or edge, v or e, to its type, $\mathcal{L}(v)$ or $\mathcal{L}(e)$. *Note that our formulation and methods are orthogonal to the format of the heterogeneous data and can be extended to support other data sources such as relational databases.*

Meta-paths, originally introduced in [37], are commonly used to extract relational graphs from KGs [13, 25, 33, 44, 46].

Definition 1 (Meta-path). *An L-hop meta-path is a sequence of node and edge types denoted as $\mathcal{M}(x_0, y_0, x_1, \ldots, x_{L-1}, y_{L-1}, x_L)$, where x_i is the type of the i-th node and y_i is the type of the i-th edge.*

Definition 2 (Matching Instance). *A matching instance M of a meta-path $\mathcal{M}$, denoted $M \triangleright \mathcal{M}$, is a sequence of nodes and edges $M(v_0, e_0, v_1, \ldots, v_{L-1}, e_{L-1}, v_L)$ in $\mathcal{G}$ satisfying:*

- $\forall i \in \{0, \ldots, L\}$, $\mathcal{L}(v_i) = x_i$.
- $\forall i \in \{0, \ldots, L-1\}$, $e_i = (v_i, v_{i+1}) \in \mathcal{E}$ *and* $\mathcal{L}(e_i) = y_i$.

When the context is clear, we use $M(v_0, v_1, \ldots, v_L)$ and M interchangeably to denote a matching instance of meta-path $\mathcal{M}$ and use $M(x_i)$ to denote the node v_i in instance M, of the node type x_i.

Definition 3 (Relational Graph). *For a given KG $\mathcal{G}$, a meta-path $\mathcal{M}$ induces a relational graph $H_{\mathcal{M}} = (V_{\mathcal{M}}, E_{\mathcal{M}})$ from $\mathcal{G}$ where:*

- *$V_{\mathcal{M}}$ contains all nodes in $\mathcal{V}$ that match x_0 in any instance of $\mathcal{M}$;*
- *$E_{\mathcal{M}}$ contains all edges $e = (u, v)$ for any two nodes $u, v \in V_{\mathcal{M}}$ such that there are $M, M' \triangleright \mathcal{M}$ in $\mathcal{G}$ with (i) $M(x_0) = u$, (ii) $M'(x_0) = v$, and (iii) $M(x_L) = M'(x_L)$.*

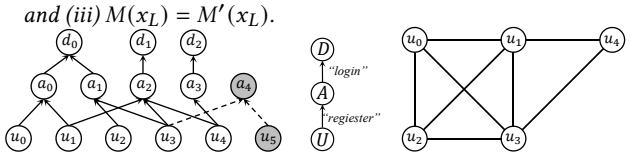

(a) Exemplary KG $\mathcal{G}$ (b) $\mathcal{M}$ (c) Relational graph $H_{\mathcal{M}}$

Figure 1: A relational graph $H_{\mathcal{M}}$ derived from a KG $\mathcal{G}$ using meta-path $\mathcal{M}(U, \text{'register'}, A, \text{'login'}, D)$. The unshaded nodes and solid edges in (a) denote the matching graph of $\mathcal{M}$.

Example 1. *Fig. 1 presents an example e-commerce KG with three node types U ("user"), A ("account"), D ("device"). Sequence (U, "register", A, "login", D) denotes a meta-path $\mathcal{M}$, which induces the relational graph $H_{\mathcal{M}}$ in Fig. 1(c). For instance, two nodes u_0 and u_2 are neighbors in $H_{\mathcal{M}}$ because there exist two instances $M = (u_0, a_0, d_0)$ and $M' = (u_2, a_1, d_0)$ of $\mathcal{M}$. More intuitively, two users u_0 and u_2 are connected since they ever login through the same device d_0.*

We denote the set of neighbors of u in $H_{\mathcal{M}}$ as $\mathcal{N}(u)$ and the *degree* of u in $H_{\mathcal{M}}$ as $N(u) = |\mathcal{N}(u)|$. Furthermore, $\Lambda = \max_{u \in H} N(u)$ denotes the maximum node degree in $H_{\mathcal{M}}$. When the context is clear, we drop the subscript $\mathcal{M}$ and denote a relational graph as $H = (V, E)$ for simplicity.

Induced Subgraph. Let $H = (V, E)$ be a relational graph and $S \subseteq V$. The induced subgraph of H *w.r.t.* S is the subgraph $H[S] = (S, E[S])$, where $E[S] = \{(u, v) \in E \mid u \in S \wedge v \in S\}$. In the rest of the paper, we abuse the notation S to also denote the subgraph it induces.

Density Metrics $\rho(\cdot)$. We define a density metric ρ for a subset S of vertices as $\rho(S) = \frac{w(S)}{|S|}$, where $w(S)$ represents the weight of the induced subgraph $H[S]$. Our proposed system supports a variety of density metrics, including those where $w(S)$ represents the number of edges (edge-density) [17], number of triangles (Δ-density) [38], or more generic functions w.r.t. node degrees [40] within $H[S]$.

The problem of *densest subgraph discovery* (DSD) over relational graphs is formally defined as follows.

Problem 1 (DSD). *Given a relational graph H (not necessarily materialized) and a density metric $\rho(\cdot)$, find a set of vertices $S^* \subseteq V$ such that $\rho(S^*)$ is maximized i.e.,*

$$S^* = \arg\max_{S \subseteq V} \rho(S).$$

Algorithm 1: `Peeling Paradigm`

Input: Relational Graph $H = (V, E)$
Output: $S \subseteq V$, such that $\rho(S)$ is maxmized
1 $S \leftarrow \emptyset, S' \leftarrow V$;
2 compute the initial *peeling coefficient* $\varphi_{S'}(u)$ for each $u \in S'$;
3 **while** $S' \neq \emptyset$ **do**
4 $v \leftarrow \arg\min_{u \in S'} \varphi_{S'}(u)$; peel v from S';
5 update $\varphi_{S'}(u)$ for each node u influenced by the peeling;
6 **if** $\rho(S') > \rho(S)$ **then** $S \leftarrow S'$;
7 return S;

For example, in Fig. 1(c), the subgraph induced by the node set $S^* = \{u_0, u_1, u_2, u_3\}$ forms the densest subgraph over the relational graph H in terms of the edge-density metric.

In this work, we focus on discovering the set of nodes S^* forming the densest subgraph instead of returning the induced subgraph $H[S^*]$. Note that after finding the set of nodes S^*, based on application requirements, $H[S^*]$ can be materialized quite efficiently by disregarding nodes outside of S^*. Exact algorithms for DSD require time-consuming max-flow computations. In this work, we follow the efficient peeling paradigm, which returns an approximated densest subgraph with theoretical guarantees.

Peeling Coefficient $\varphi_S(u)$. The peeling coefficient function, denoted by $\varphi_S(u)$, quantifies a node's marginal contribution to the density of the induced subgraph $H[S]$. Its calculation is dependent on the chosen density metric. We define $\varphi_S(u)$ as follows:

$$\varphi_S(u) = w(S) - w(S \setminus \{u\}) \quad (1)$$

When the context is clear, we drop S and denote the peeling coefficient as $\varphi(u)$ for simplicity.

Peeling Paradigm (Algorithm 1). The peeling paradigm is a general iterative approach for DSD. Given a relational graph H, it begins by computing the initial peeling coefficient of each node in H (Line 2) and then obtains a sequence of subgraphs by peeling vertices iteratively (Line 3–6). In each iteration, it peels the node with minimum *peeling coefficient* (Line 4), updates the peeling coefficient for the set of nodes whose peeling coefficient is influenced by the peeling (Line 5), and maintains the subgraph with largest density (Line 6). Finally, the subgraph of the largest density is returned (Line 7). The *peeling coefficient* is determined by the density metric to achieve good approximations of the optimal.

The time overhead of the peeling paradigm mainly comes from two parts. The first part is initializing the peeling coefficient of each node $u \in V$. The second part is updating the peeling coefficient for nodes that are influenced by the peeling of the node with smallest peeling coefficient in each iteration. Although the peeling algorithm has a linear number of iterations, it can still be time-consuming for certain density metrics. For example, Δ-density [38] requires computing the number of triangles containing each node which costs $O(n^{2.376})$ time, and the number of nodes influenced by peeling at each peeling iteration can be significant for distance-generalized metrics [7]. As discussed in Sec. 3.2, our proposal can not only avoid the materialization stage but also accelerate the peeling iterations by utilizing sketches for efficiently estimating and updating the peeling coefficients.

2.2 Related Work

Relational Graph Materialization. A straightforward solution of our problem is to first materialize the relational graph and then execute DSD algorithms over it. Instead of enumerating all instances of meta-paths, there has been a line of works on improving the efficiency for relational graph materialization. For example, Chatzopoulos et al. [11] proposed a method to enumerate instances of different meta-paths through workload sharing. Guo et al. [18] proposed the algorithm to materialize relational graphs by boolean matrix multiplication, specially optimized for graphs with locally dense regions. The generic worst-case optimal join [3, 15, 32, 39] algorithm can also be used for relational graph materialization through efficient traversal of meta-path instances avoiding duplicate visit of nodes in multiple meta-path instances. Our experiments (Sec. 5.2) reveal that the materialization costs remain time-consuming and are the bottleneck for DSD in relational graphs.

Densest Subgraph Discovery. There is a rich literature on the problem of DSD. Exact DSD algorithms involve solving a max-flow [14, 17] or linear programming [10] problem, which is not scalable to large graphs. Thus, the peeling paradigm, which is efficient with approximation guarantees, has been widely adopted in the literature. Charikar [10] proposed the peeling algorithm for edge-density, which iteratively removes nodes with smallest degree and returns the subgraph with largest edge-density generated during the peeling iterations. Instead of removing one node in each peeling iteration, Bahmani et al. [4] proposed to remove all nodes with degree less than $2(1+\epsilon)\rho$ at each peeling iteration and prove that this algorithm achieves a solution of $2(1+\epsilon)$-approximation. Boob et al. [8] proposed the multi-round peeling algorithm, which obtains the densest subgraph by iteratively removing the node with the smallest load, where the load of a node in each round is the sum of its induced degree and its load in previous round. The peeling paradigm has also been extended to other density metrics. Tsourakakis et al. [38] modeled the graph density as the number of k-cliques contained in the graph and showed that the peeling algorithm of repeatedly removing the node contained in the smallest number of corresponding cliques achieves k-approximation.

All these works assume that the relational graph is already materialized and thus cannot scale to large heterogeneous data sources owing to the requirement of materializing the relational graph.

Community Search over Heterogeneous Information Networks (HIN). Recently, several works have focused on the community search problem over HINs based on meta-paths.

Fang et al. [13] proposed to reveal $(k, \mathcal{M})$-core from HINs, which is equivalent to the k-core in the relational graph induced by meta-path $\mathcal{M}$. The algorithm dynamically maintains k neighbors for each node in the relational graph through meta-path instances and removes nodes with less than k neighbors iteratively. Yang et al. [44] introduced the $(k, \mathcal{M})$-Btruss and $(k, \mathcal{M})$-Ctruss models for community search in KGs. The $(k, \mathcal{M})$-Btruss is equivalent to the k-truss in the relational graph induced by $\mathcal{M}$, whereas $(k, \mathcal{M})$-Ctruss considers the overlaps between meta-path instances and does not correspond to existing models of cohesive subgraphs in the relational graphs. Jiang et al. [23] studied the nested meta-path core (k, Ψ)-core, which aims at finding a subgraph that is $(k, \mathcal{M})$-core for each meta-path $\mathcal{M} \in \Psi$.

The above methods focus on discovering subgraphs conforming to certain topological community models with strict topological constraints and can overlook relevant subgraphs with complex topological structures [45]. Instead, our work focuses on finding the subgraph optimizing the density metric, which is more flexible than topology-driven community search methods.

Strouthopoulos and Papadopoulos [35] studied the discovery of k-cores in hidden networks, where the existence of any edge can only be decided via a *probe operation*. However, this work also aims at finding subgraphs conforming to the k-core model. Besides, their method cannot handle large relational graphs since the probe operations are time-consuming over relational graphs, as it involves bread-first search (BFS) on the matching graph.

3 THE SCANS SYSTEM

In this section, we first present an overview of our proposed SCANS system and APIs. Subsequently, we describe in detail the sketch-peeling algorithm, which constructs and maintains the sketches utilized in the SCANS system.

3.1 Overview of SCANS and APIs

We observe that the peeling paradigm for DSD only requires the *peeling coefficient* of each node for node removal and the densities of the sequence of generated subgraphs to determine the output subgraph. Based on this, our SCANS system follows the peeling paradigm and avoids the materialization of the relational graphs by utilizing persistent sketches to efficiently estimate the peeling coefficients and subgraph densities during the peeling iterations.

Crafting the complete SCANS system for different density metrics can be cumbersome for data engineers, given the significant effort required to construct and maintain the sketches within the system. SCANS streamlines this endeavor and provides a set of interfaces to efficiently implement peeling algorithms for different density metrics. This allows data engineers to concentrate on selecting the best density metric and the corresponding peeling coefficient for their particular real-world application.

```
class SCANS{
    virtual double coefficient(int v, sketchSet K);
    virtual double density(vector<int> S, sketchSet K);
    // S represents the subgraph induced by nodes in it
    double val(sketch k);
}
```

Listing 1: APIs of SCANS

Application Programming Interfaces (APIs). Listing 1 presents the key APIs in SCANS system through which users can deploy the SCANS system for DSD based on various density metrics over relational graphs. Parameter `sketchSet K` contains the set of sketches corresponding to each node in V, whereas `sketch k` denotes one specific sketch within `K`.

- `coefficient()` estimates the *peeling coefficient* for node `v` utilizing sketches in `K`. This API is called when computing the initial peeling coefficients as well as updating the peeling coefficient of influenced nodes after each removal during peeling iterations.
- `density()` estimates the density of the given subgraph `S` utilizing the sketches of nodes in `S` according to density metrics implemented by the user. This API is called to estimate the density of the sequence of subgraphs generated during peeling iterations.
- `val()` gives the estimation of the cardinality of the collection represented by the sketch `k`. This API can be used by users for implementing the APIs `coefficient()` and `density()`.

3.2 Implementation of SCANS

We first review the KMV sketch which is used in SCANS. It was initially proposed for distinct value estimation [5, 6].

Definition 4 (KMV Sketch). *Given an item collection $C = \{o_0, o_1, ..., o_{|C|}\}$ and an integer $k > 0$, the KMV (k-th Minimum Value) sketch $\mathcal{K}(C)$ is constructed by sampling an independent uniform random number from $(0, 1)$ for each item in C and maintaining the k smallest random numbers. The set of random numbers generated for all items in C is called the* basis *of the KMV sketch. The cardinality of C is estimated as $\widetilde{|C|} = \frac{k}{\mathbb{E}[\zeta]} - 1$, where ζ is a random variable corresponding to the largest number in $\mathcal{K}(C)$ and $\mathbb{E}[\zeta]$ is the expectation of ζ.*

Properties of KMV. We adopt the KMV sketches in SCANS due to the following desirable properties:

- *Efficiency:* The KMV sketches can be constructed for each node in the relational graph efficiently from external KGs.
- *Persistency:* The KMV sketches can be maintained persistently during peeling iterations efficiently.
- *Flexibility:* The KMV sketches are compatible with multiple set operations [6] so they can support the estimation of complex peeling coefficients and subgraph densities.

Sketch-Peeling Algorithm. Next, we present the sketch-peeling algorithm , which forms the core of SCANS. It efficiently constructs and maintains the KMV sketches for the neighborhood of each node in the relational graph without materialization and utilizes the sketches for DSD.

Sketch Construction. The naïve approach is to first obtain the neighborhood of each node in the relational graph H and then construct the KMV sketches as described in Def. 4. In particular, the neighborhood of each node in H can be obtained by propagating nodes in the *matching graph*, defined next.

Definition 5 (matching graph). *Given a KG $\mathcal{G}$ and a meta-path $\mathcal{M}(x_0, y_0, x_1, \ldots, x_{L-1}, y_{L-1}, x_L)$, the* matching graph *of $\mathcal{M}$ over $\mathcal{G}$ is a* multi-level *graph $\mathcal{G}^*(\mathcal{V}^*, \mathcal{E}^*)$ with node set $\mathcal{V}^* = \bigcup_{0 \le i \le L} \mathcal{V}_i$ and edge set $\mathcal{E}^* = \bigcup_{0 \le i < L} \mathcal{E}_i$, where $\mathcal{V}_i$ is the set of nodes of type x_i contained in any matching instance of $\mathcal{M}$ and $\mathcal{E}_i$ consists of all edges of type y_i that connect nodes between $\mathcal{V}_i$ and $\mathcal{V}_{i+1}$.*

Definition 6 (Successors & Predecessors). *For each node $u \in \mathcal{V}_i$, we use $\mathcal{V}^+(u)$ to denote the nodes in $\mathcal{V}_{i+1}$ connected with u through edge type y_i, i.e., the* successors *of u in $\mathcal{G}^*$; similarly we use $\mathcal{V}^-(u)$ to denote the nodes in $\mathcal{V}_{i-1}$ connected with u through edge type y_{i-1}, i.e., the* predecessors *of u in $\mathcal{G}^*$.*

Example 2. *The unshaded nodes and solid edges in Fig. 1(a) denote the matching graph of meta-path $\mathcal{M}$ in Fig. 1(b). Nodes a_4 and u_5 are not contained within the matching graph because they are not contained in any matching instance of $\mathcal{M}$. Thus, we have $\mathcal{V}_0 =$*

$\{u_0, u_1, u_2, u_3, u_4\}$ *and* $\mathcal{V}_1 = \{a_0, a_1, a_2, a_3\}$. *The set of predecessors of* a_2 *is* $\mathcal{V}^-(a_2) = \{u_1, u_3, u_4\}$ *and the set of successors of* u_3 *is* $\mathcal{V}^+(u_3) = \{a_1, a_2\}$.

By propagating all nodes in $\mathcal{V}_0$,[1] along the edges of the matching graph from $\mathcal{V}_0$ to $\mathcal{V}_L$ (*forward propagation*) and then from $\mathcal{V}_L$ to $\mathcal{V}_0$ (*backward propagation*), each node in $\mathcal{V}_0$ will receive all its neighbors in H. However, explicitly obtaining the whole neighborhood of each node can lead to a prohibitive time complexity of $O(|V| \cdot |\mathcal{E}^*|)$ since each node in $\mathcal{V}^*$ potentially retains all the nodes it has received and then propagates these nodes to its successors (during forward propagation) or predecessors (during backward propagation) through the edges in $\mathcal{G}^*$.

Fortunately, this prohibitive complexity can be circumvented by utilizing the fact that the KMV sketch construction does not require all neighbors of each node. Instead, it only requires a subset of a node's neighbors corresponding to the smallest k random numbers in the KMV sketch basis. Thus, each node in $\mathcal{V}^*$ only needs to preserve and propagate at most k nodes[2] received during the propagation process.

Specifically, we begin by generating a random number for each node $v \in V$, denoted $r(v)$, as the basis of the KMV sketch. Each node in $\mathcal{V}_{i-1}$ propagates the random numbers it maintains to its successors. Each node in $\mathcal{V}_i$ will retain the k-smallest random numbers it receives. When each node in $\mathcal{V}_L$ has received its random numbers, they will propagate the random numbers back to nodes in $\mathcal{V}_0$, still retaining the k-smallest random numbers at each node in $\mathcal{V}^*$. Finally, each node in $\mathcal{V}_0$ will receive k random numbers forming the KMV sketch for its neighborhood. This sketch construction process is presented as Function `construct()` in Alg. 2, where the operator $\oplus$ extracts the k smallest random numbers from the union of random number collections.

Lazy Sketch Maintenance. We can use the KMV sketches as constructed above to estimate the peeling coefficient $\varphi(v)$ for each node $v \in V$ and the current density $\rho(H)$. However, during the peeling iterations, nodes are iteratively removed and the remaining subgraph is changed continuously. Thus, the KMV sketches can become outdated. A naïve solution is to reconstruct the KMV sketches at each peeling iteration. However, this approach is expensive since it requires reconstructing the KMV sketches $O(V)$ times.

To this end, we propose a *lazy sketch maintenance* approach for efficient maintenance of KMV sketches during peeling iterations. At each peeling iteration, when a node v is removed, we can easily maintain the KMV sketches for nodes in the remaining subgraph by removing the random number $r(v)$ corresponding to v from the KMV sketches. Specifically, for each KMV sketch of size k' containing $r(v)$, we will obtain a KMV sketch of size $k' - 1$ without $r(v)$ after the peeling iteration. Since the original KMV sketch before maintenance retains the k' smallest random numbers corresponding to nodes in the neighborhood, after removing the random number $r(v)$ from the KMV sketch, it still retains the $k' - 1$ smallest random numbers corresponding to nodes in the remaining neighborhood. However, since the accuracy of the KMV sketch is proportional to its size, the *lazy sketch maintenance* can potentially deteriorate the effectiveness of the KMV sketches. To alleviate this problem, we reconstruct the KMV sketches whenever we find they not effective enough for estimation. More precisely, we set a threshold k^- and reconstruct the KMV sketches whenever their size falls below k^-. This lazy sketch maintenance is presented as Function `update()` in Alg. 2.

Sketch-based Peeling. Alg. 2 gives the pseudocode for the sketch-peeling algorithm. It receives a KG $\mathcal{G}$, a meta-path $\mathcal{M}$, the number of sketches $\theta \in \mathbb{Z}^+$ and the sketch size bounds $k, k^- \in \mathbb{Z}^+$ as input, and returns a subset S of V maximizing the density of $H[S]$ for DSD. The algorithm takes the average of estimations obtained through θ KMV sketches for each node in H to achieve good approximation guarantees for peeling coefficients and subgraph densities. It first initializes the empty buffer $\mathcal{K}$ for storing the KMV sketches and array I indicating the index of sketches to be constructed and then constructs the θ sketches (Lines 1–2). Then, the peeling iterations proceed until only one node remains (Lines 3–9). In each iteration, the algorithm selects and removes the node with the smallest peeling coefficient by calling API `coefficient` (Lines 4–5). Then, the algorithm calls procedure `update` to perform lazy maintenance of the sketches and obtains the indices I of sketches that need to be reconstructed (Line 6). Then it reconstructs the sketches indicated in I over the current remaining subset S' (Line 7). At the end of each iteration, API `density` is called to estimate the density of $H[S']$ (Line 8) and the subset that induces larger density is maintained in S (Line 9). Finally, the subset S inducing the largest density obtained during the peeling iterations is returned as the result (Line 10).

Example 3. *Fig. 2 illustrates the sketch-peeling algorithm that induces densest subgraph based on edge-density over the relational graph in Fig. 1(c) with sketch size bounds set to* $k = 2$ *and* $k^- = 1$. *First, the sketches are constructed by propagating the random numbers forward (Fig. 2(a) left) and backward (Fig. 2(b) right) along the matching graph. Fig. 2(b) denotes the first and second peeling iteration, where node* u_4 *and* u_2 *with peeling coefficient* $\varphi(u_4) = \frac{2}{0.6} - 1 = 2.33$ *and* $\varphi(u_2) = \frac{2}{0.4} - 1 = 4$ *are removed respectively. The subsets* $S_1 = \{u_0, u_1, u_2, u_3\}$ *and* $S_2 = \{u_0, u_1, u_3\}$ *with estimated density* $\rho(S_1) = \frac{(\frac{2}{0.4}-1)\cdot 4}{2\cdot 4} = 2$ *and* $\rho(S_2) = \frac{(\frac{1}{0.4}-1)\cdot 3}{2\cdot 3} = 0.75$ *are generated in the peeling iterations. The sketches are reconstructed as depicted in Fig. 2(c). The third and fourth peeling iterations are presented in Fig. 2(d), where node* u_0 *and* u_3 *with peeling coefficient* $\varphi(u_0) = \frac{2}{0.6} - 1 = 2.33$ *and* $\varphi(u_3) = \frac{2}{0.6} - 1 = 2.33$ *are removed, resulting in subset* $S_3 = \{u_1, u_3\}$ *with density* $\rho(S_3) = \frac{(\frac{2}{0.6}-1)\cdot 2}{2\cdot 2} = 1.167$. *Thus, subset* S_1 *is returned as the largest density subgraph.*

Theorem 1. *The time complexity of Alg. 2 is* $O(k(\theta + \theta^*)(|\mathcal{E}^*| + |V|f(k) + |V|\log|V|))$, *where* $f(k)$ *denotes the time complexity for peeling coefficient estimation using KMV sketches and* θ^* *denotes the total number of sketches reconstructed during the peeling iterations.*

Proof. There are mainly two contributors to the time complexity of the sketch-peeling algorithm. First, the algorithm needs to construct the KMV sketches. The construction of KMV sketches requires propagating at most k random numbers over the matching graph with $|\mathcal{E}^*|$ edges, which takes $O(k \cdot |\mathcal{E}^*|)$ time. The algorithm constructs θ KMV sketches at the beginning of the algorithm and reconstructs θ^* sketches that are disabled by node removals during

[1] Note that $\mathcal{V}_0$ equals the node set V of relational graph H.
[2] Random numbers, to be precise.

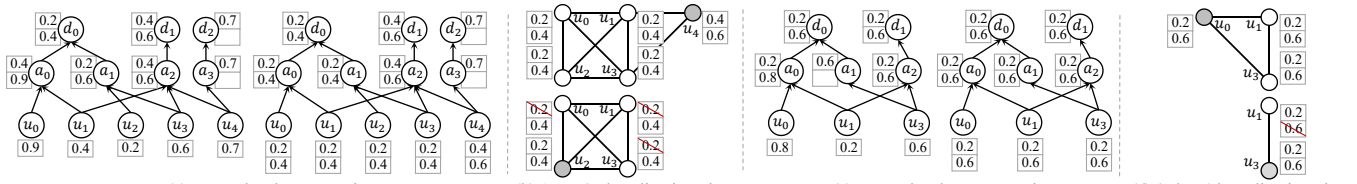

(a) KMV sketch construction (b) 1st & 2nd peeling iterations (c) KMV sketch reconstruction (d) 3rd & 4th peeling iterations

Figure 2: Sketch-peeling algorithm with $k = 2$ and $k^- = 1$. Shaded nodes in subfigures (b) and (d) denote the nodes removed in the peeling iteration and the elements in KMV sketches with red strikethrough are the random numbers corresponding to the removed nodes. Note that subgraphs in (b) and (d) are only for demonstration and not materialized in our algorithm.

Algorithm 2: Sketch-based Peeling

Input: KG $\mathcal{G}$, meta-path $\mathcal{M}$, number of sketches θ, KMV sketch size bounds k, k^-
Output: A set of nodes $S \subseteq V$

$S \leftarrow \emptyset, \rho \leftarrow 0, S' \leftarrow V, I \leftarrow \{1, 2, 3, ..., \theta\}$ and $\mathcal{K}[][] \leftarrow \emptyset$;
construct($\mathcal{K}, V, I$);
while $|S'| > 1$ **do**
  $v \leftarrow \arg\min_{u \in S'}$ coefficient$(u, \mathcal{K})$;
  remove v from S';
  $I \leftarrow$update$(\mathcal{K}, v)$;
  construct$(\mathcal{K}, S', I)$;
  $\rho' \leftarrow$density$(S', \mathcal{K})$;
  if $\rho' > \rho$ **then** $S \leftarrow S', \rho \leftarrow \rho'$;
return S;
Function construct$(\mathcal{K}, S, I)$:
  for $\tau \in I$ **do**
    if $u \in S$ **do** $\mathcal{K}[u][\tau] \leftarrow$ Rand$(0, 1)$;
    for $i = 1$ **to** L **do**
      for $u \in \mathcal{V}_i$ **do** $\mathcal{K}[u][\tau] \leftarrow \oplus_{v \in \mathcal{V}^-(u)} \mathcal{K}[v][\tau]$;
    for $i = L - 1$ **to** 0 **do**
      for $u \in \mathcal{V}_i$ **do** $\mathcal{K}[u][\tau] \leftarrow \oplus_{v \in \mathcal{V}^+(u)} \mathcal{K}[v][\tau]$;
Function update$(\mathcal{K}, u)$:
  $I \leftarrow \emptyset$;
  for $\tau = 1$ to θ **do**
    for $v \in S'$ **do**
      remove $r_\tau(v)$ from $\mathcal{K}[v][\tau]$;
      if $|\mathcal{K}[v][\tau]| < k^-$ **then** $I \leftarrow I \cup \{\tau\}$;
  return I;

peeling iterations. Thus, the time complexity of sketch construction is $O((\theta + \theta^*)k \cdot |\mathcal{E}^*|)$. Then, at each peeling iteration, the algorithm updates the KMV sketches by removing from $\mathcal{K}$ the random number corresponding to the removed node, re-estimates the peeling coefficients with updated KMV sketches, and maintains the min-heap for identifying the node with smallest peeling coefficient. Since $(\theta + \theta^*)$ KMV sketches are constructed for each node, at most $O(k|V|(\theta + \theta^*))$ KMV sketch updates will be performed. For each KMV sketch update, it will takes $f(k)$ time to re-estimate the peeling coefficient and $O(\log |V|)$ time to maintain the min-heap. The KMV sketch update itself can be performed in $O(1)$ utilizing an inverted list from random numbers to KMV sketches. Thus, the time complexity is $O(k|V|(\theta+\theta^*)(f(k)+\log|V|))$. Therefore, the total time complexity of the sketch-peeling algorithm is $O(k(\theta + \theta^*)(|\mathcal{E}^*| + |V|f(k) + |V| \log |V|))$. □

The time complexity of Alg. 2 is significantly influenced by the number θ of sketches constructed as well as the number θ^* of sketches reconstructed due to node removals during the peeling iterations. In Sec. 4, we theoretically bound the value of θ in the worst case so that our method achieves approximation guarantees for edge-density and triangle density. The value of θ^*, which is closely related to the specific structure of the relational graph, is often small as indicated by our experiments. We leave the theoretical study of θ^* as a future work. Function $f(k)$ is determined by the target density metric. As discussed in Sec. 4, for edge-density, we have $f(k) = O(k)$; for triangle-density, we have $f(k) = O(k^2)$.

Theorem 2. *The space complexity of Alg. 2 is* $O(k\theta|\mathcal{V}^*| + |\mathcal{E}^*|)$.

Proof. The firsts term $O(k\theta|\mathcal{V}^*|)$ is the memory consumption of KMV sketches and the second term $O(|\mathcal{E}^*|)$ is the memory consumption of the matching graph $\mathcal{G}^*$. □

4 DEPLOYMENT OF SCANS SYSTEM

In this section, we deploy the SCANS system for two common density metrics to demonstrate the effectiveness and flexibility of SCANS. For each density metric, we first give the implementation of APIs for peeling coefficient and subgraph density estimation and then conduct a theoretical analysis of the sketch-based algorithm.

In general, our SCANS system can support any density metric that can be computed by the cardinality of node neighborhoods or cardinality of set operations (union, intersection or difference supported by KMV sketches [6]) of node neighborhoods. For example, edge density, p-mean density [40] and densities with convex or concave size functions [24] are computed by the cardinality of node neighborhoods; for triangle-density, the common neighbors are computed through intersections of node neighborhoods.

4.1 Edge-density $\rho_e(S)$

We first deploy the SCANS system over edge-density metric, first proposed by Goldberg [17]:

Definition 7 (Edge-density). *Given a graph $S = (V_S, E_S)$, its edge-density is defined as* $\rho_e(S) = \frac{|E_S|}{|V_S|}$.

Charikar [10] shows that by using degree $N(v)$ of each node v as the *peeling coefficient*, the peeling algorithm, run on a materialized relational graph, can achieve a 2-approximation guarantee for the densest subgraph based on edge-density. Class EdgeSCANS in

Listing 2 implements the corresponding peeling algorithm in the SCANS system. The API `coefficient(v, K)` performs function `val` on the KMV sketch of node `v` to obtain an estimation of its degree (Line 3). For each subgraph `S` generated during peeling iterations, the API `density(S, K)` estimates its edge-density as the average degree of each node in `S` divided by 2 (Lines 6-8).

```
1  class EdgeSCANS: public SCANS{
2      double coefficient(int v, sketchSet K) {
3          return val(K[v]);
4      }
5      double density(vector<int> S, sketchSet K){
6          double den;
7          for(int v: S) den += coefficient(v, K);
8          return den / (S.size() * 2);
9      }
10 }
```

Listing 2: Edge-densest Subgraph Discovery in SCANS

Theoretical Analysis. We extend Charikar's result and prove that the sketch-based algorithm gives a $2(1+\epsilon)$-approximation of DSD with high probability (w.h.p.). Let S_t denote the subgraph generated at the t-th peeling iteration.

Lemma 1. *For any $0 \le t < |V|$, we have $\frac{\rho_e(S_t)}{1+\delta} \le \widetilde{\rho}_e(S_t) \le \frac{\rho_e(S_t)}{1-\delta}$ holds w.p. at least $(1-p)$, provided $\theta = \Theta(\frac{\Lambda}{\delta k}\log\frac{|V|}{p})$.*

Proof Sketch. We first show that for any $\delta, p \in (0,1)$ and any node $v \in S_t$, if $\theta = \Theta(\frac{\Lambda}{\delta k}\log\frac{1}{p})$, then $(1-\delta)\cdot N_{S_t}(v) \le \widetilde{N}_{S_t}(v) \le (1+\delta)\cdot N_{S_t}(v)$ holds w.p. at least $1-p$. Then, by using the union bound over all nodes in S_t, we have $\rho_e(S_t) = \frac{\sum_{u\in S_t} N_{S_t}(u)}{2\cdot|V_{S_t}|} \ge \frac{\sum_{u\in S_t}\widetilde{N}_{S_t}(u)}{2(1+\delta)|V_{S_t}|} = \frac{\widetilde{\rho}_e(S_t)}{1+\delta}$ and similarly $\rho_e(S_t) \le \frac{\sum_{u\in S_t}\widetilde{N}_{S_t}(u)}{2(1-\delta)|V_{S_t}|} = \frac{\widetilde{\rho}_e(S_t)}{1-\delta}$ holds simultaneously w.p. $(1-p)$. □

Theorem 3. *Let S denote the subgraph returned by Alg. 2, we have $\rho_e(S) \ge \frac{\rho_e(S^*)}{2(1+\epsilon)}$ w.p. at least $(1-p)$, provided $\theta = \Theta(\frac{\Lambda}{\epsilon k}\log\frac{|V|}{p})$.*

Proof. For a node $v \in S^*$, since S^* is the densest subgraph of H, we have $\rho_e(S^*) \ge \rho_e(S^* - \{v\})$, i.e., $\frac{|E_{S^*}|}{|V_{S^*}|} \ge \frac{|E_{S^*}| - N_{S^*}(v)}{|V_{S^*}|-1}$. Thus,

$$N_{S^*}(v) \ge \frac{|E_{S^*}|}{|V_{S^*}|} = \rho_e(S^*). \tag{2}$$

Consider the first iteration in which a node $u \in S^*$ is going to be removed by Alg. 2 and let S_t denote the subgraph just before u is removed. According to Lemma 1, for any node $v' \in S_t$, we have

$$N_{S_t}(v') \ge \frac{\widetilde{N}_{S_t}(v')}{(1+\delta)} \ge \frac{\widetilde{N}_{S_t}(u)}{(1+\delta)} \ge \frac{(1-\delta)}{(1+\delta)}\cdot N_{S_t}(u) \tag{3}$$

holds w.p. at least $(1-p)$, given $\theta = \Theta(\frac{\Lambda}{\delta k}\log\frac{1}{p})$. The second inequality in (3) holds since the nodes in H are removed in the ascending order of estimated degrees. Then, by applying union bounds over all nodes in S_t, we have

$$\rho_e(S_t) = \frac{\sum_{v'\in S_t} N_{S_t}(v')}{2|V_{S_t}|} \ge \frac{(1-\delta)\sum_{v'\in S_t} N_{S_t}(u)}{2(1+\delta)|V_{S_t}|} \ge \frac{(1-\delta)}{2(1+\delta)}\rho_e(S^*) \tag{4}$$

holds with probability at least $(1-p)$ provided $\theta = \Theta(\frac{\Lambda}{\delta k}\log\frac{|V|}{p})$. The last inequality holds since $N_{S_t}(u) \ge \rho_e(S^*)$ according to Eq. 2.

Let $S = \arg\max_{0\le t\le|V|}\widetilde{\rho}_e(S_t)$ denote the subgraph returned by Alg. 2. Then according to Lemma 1, we have

$$\rho_e(S) \ge (1-\delta)\widetilde{\rho}_e(S) \ge (1-\delta)\widetilde{\rho}_e(S_t) \ge \frac{1-\delta}{1+\delta}\rho_e(S_t) \ge \frac{(1-\delta)^2}{2(1+\delta)^2}\rho_e(S^*) \tag{5}$$

For any $\epsilon \in (0,1)$, we can set $\delta = (3-2\sqrt{2})\epsilon < 1 + \frac{2-2\sqrt{1+\epsilon}}{\epsilon}$, i.e., $\theta = \Theta(\frac{\Lambda}{\epsilon k}\log\frac{|V|}{p})$. So we have $\frac{1}{2(1+\epsilon)} < \frac{(1-\delta)^2}{2(1+\delta)^2}$ and thus $\rho_e(S) > \frac{\rho_e(S^*)}{2(1+\epsilon)}$ w.p. at least $(1-p)$. The theorem follows. □

The time complexity of edge-density optimization with the SCANS framework is $O(k(\theta+\theta^*)(|\mathcal{E}^*|+|V|k+|V|\log|V|))$ according to Theorem 1 since peeling coefficient estimation requires $f(k) = O(k)$ time to find the largest random number in the KMV sketch. In practice, we find that θ^* is small when optimizing the edge-density metric (see Sec. 5.2). The intuition behind this is the following. The KMV sketch of a node will only be updated during those peeling iterations when the removed node happens to correspond to a random number in the KMV sketch. For a node v with large degree, the update of its KMV sketch will only take place with a small probability $k/N(v)$ due to its large neighborhood. On the other hand, for nodes with small degrees, since nodes are removed in the ascending order of degrees, these nodes will be removed during early peeling iterations and thus also do not require sketch reconstruction w.h.p.

4.2 Triangle-density $\rho_\Delta(S)$

We next consider employing the SCANS framework for the optimization of triangle-density [38], which is the average number of triangles containing a vertex in a given induced subgraph.

Definition 8 (Δ-density). *For a graph $S = (V_S, E_S)$, its triangle-density, also denoted as Δ-density, is $\rho_\Delta(S) = \frac{\Delta(S)}{|V_S|}$, where $\Delta(S)$ is the number of triangles in S.*

Tsourakakis [38] shows that by using the number of triangles containing the node v as the *peeling coefficient*, denoted as $\Delta(v)$, the peeling algorithm can achieve a 3-approximation guarantee for triangle-density optimization. Thus, to deploy our SCANS system on triangle-density metric, we need to estimate the number of triangles containing each node based on the sketches. The following lemma indicates that the peeling coefficient $\Delta(v)$ can be computed based on the neighborhood of v.

Lemma 2. *For any node $v \in S$, we have $\Delta(v) = \frac{\sum_{u\in N(v)}\Delta(v,u)}{2}$, where $\Delta(v,u)$ denotes the support (u,v), i.e., the number of triangles containing the edge (u,v).*

Based on Lemma 2 and the Horvitz-Thompson [20] estimator, the peeling coefficient $\Delta(v)$ can be estimated through Monte-Carlo simulation. Specifically, if we uniformly sample a set of nodes C from $\mathcal{N}(v)$, the peeling coefficient $\Delta(v)$ can be estimated as $\frac{1}{2}\sum_{u\in C}\frac{\Delta(u,v)}{\frac{|C|}{N(v)}} = \frac{N(v)}{2|C|}\sum_{u\in C}\Delta(u,v)$, where $\frac{|C|}{N(v)}$ is the probability of sampling specific node u from $\mathcal{N}(v)$. The challenge is that since we do not materialize the relational graph, we cannot obtain the exact value of $N(v)$ and $\Delta(u,v)$ for certain sampled neighbor u.

To this end, we provide a novel estimator for $\Delta(v)$ by replacing the terms $N(v)$ and $\Delta(u,v)$ in the Horvitz-Thompson estimator

with corresponding approximate values estimated through the KMV sketches. Specifically, note that the KMV sketch $\mathcal{K}(v)$ of node v offers a uniform sample of its neighbors of size k naturally, i.e., the set of nodes corresponding to the random numbers in $\mathcal{K}(v)$. For simplicity, we abuse the notation and use $u \in \mathcal{K}(v)$ to denote a node u that is sampled into the KMV sketch. Then, for each node $u \in \mathcal{K}(v)$, since the support of edge (v,u) equals the number of common neighbors of u and v, i.e., $\Delta(u,v) = |\mathcal{N}(u) \cap \mathcal{N}(v)|$, we can estimate $\Delta(u,v)$ for each node $u \in \mathcal{K}(v)$ by taking the intersection of KMV sketches $\mathcal{K}(u)$ and $\mathcal{K}(v)$. Formally, we provide the following estimator for $\Delta(v)$:

$$\tilde{\Delta}(v) = \frac{\tilde{N}(v) \cdot \sum_{u \in \mathcal{K}(v)} \tilde{\Delta}(u,v)}{2k} \tag{6}$$

where $\tilde{N}(v)$ is the degree estimate of v based on the KMV sketch $\mathcal{K}(v)$. Since the KMV sketch provides a uniform sample of size k from $\mathcal{N}(v)$, the probability for a certain node u to be sampled is estimated as $\frac{k}{|N(v)|}$. Each $\tilde{\Delta}(u,v)$ is an estimate of $\Delta(u,v)$ obtained by taking the intersection of $\mathcal{K}(v)$ and $\mathcal{K}(u)$.

Next, to obtain the estimator for the triangle density of a subgraph S generated during the peeling iterations, observe that $\rho_\Delta(S) = \frac{\sum_{v \in S} \Delta(v)}{3}$. Then the estimator for $\rho_\Delta(S)$ can be obtained as:

$$\tilde{\rho}_\Delta(v) = \frac{\sum_{v \in S} \tilde{\Delta}(v)}{3} \tag{7}$$

```
1  class TriangleSCANS: public SCANS{
2     double coefficient(int v, sketchSet K) {
3           double d = val(K[v]), t = 0, s = 0;
4           for(int u: K[v].nbr()) t += val(K[u] & K[v]);
5           return (t * d) / (K[v].size() * 2);
6     }
7     double density(vector<int> S, sketchSet K) {
8           double t = 0;
9           for(int v: S) t += coefficient(v, K);
10          return t / (S.size() * 3);
11    }
12 }
```

Listing 3: Triangle-densest Subgraph Discovery in SCANS

Listing 3 gives the implementation of the SCANS system for triangle-densest subgraph discovery. The operator & (Line 4) is reloaded as the intersection between two sketches. The function `coefficient(v, K)` first estimates the degree of node v (Line 3), and then for each neighbor of v sampled within the KMV sketch `K[v]`, it counts the number of triangles containing edge (u,v) based on KMV sketch intersections and records the total number of triangles in variable `t` (Line 4). Finally, the estimator is computed according to Eq. 6 and returned (Line 5). The API `density(S, K)` is implemented to estimate the triangle-density of a given subgraph `S` according to Eq. 7 by calling `coefficient` for each node in `S`.

Theoretical Analysis. We note that the intersection operation required by estimation of $\Delta(v)$ breaks the probabilistic bounds of our estimators. We can nevertheless prove that the estimator in Eq. 6 and 7 provide an unbiased estimation of the *peeling coefficient* of each node accessed and triangle-density of each subgraph generated during the peeling iterations.

Theorem 4. *Given any node $v \in S_t$, $\tilde{\Delta}(v)$ is an unbiased estimator of $\Delta(v)$, i.e., $\Delta(v) = \mathbb{E}[\tilde{\Delta}(v)]$.*

Proof. By obtaining estimates for the degree $\tilde{N}(v)$ and support of edge (u,v) $\tilde{\Delta}(u,v)$ using two different KMV sketches of node v with independent bases, we can ensure that the estimation $\tilde{N}(v)$ and $\sum_{u \in \mathcal{K}(v)} \tilde{\Delta}(u,v)$ are independent of each other. Thus, we have

$$\begin{aligned} \mathbb{E}[\tilde{\Delta}(v)] &= \mathbb{E}[\mathbb{E}[\tilde{\Delta}(v)]] = \mathbb{E}[\frac{\mathbb{E}[\tilde{N}(v)] \cdot \mathbb{E}[\sum_{u \in \mathcal{K}(v)} \tilde{\Delta}(u,v)]}{2k}] \\ &= \mathbb{E}[\frac{N(v) \cdot \sum_{u \in \mathcal{K}(v)} \Delta(u,v)}{2k}] = \Delta(v) \end{aligned} \tag{8}$$

The second equality is due to the independence between $\tilde{N}(v)$ and $\sum_{u \in \mathcal{K}(v)} \tilde{\Delta}(u,v)$; the third equality is due to the unbiasedness of estimation based on the KMV sketch according to [6]; the last equality is due to the Horvitz–Thompson estimator. □

Corollary 1. *For any subgraph S_t generated during the peeling iteration, we have $\tilde{\rho}_\Delta(S_t)$ is an unbiased estimator of $\rho_\Delta(S_t)$, i.e., $\rho_\Delta(S_t) = \mathbb{E}[\tilde{\rho}_\Delta(S_t)]$.*

Proof. This corollary follows trivially from the addition rule of expectation and the unbiasedness of the peeling coefficient estimator in Theorem 4. □

The time complexity of triangle-density DSD with SCANS is $O(k(\theta + \theta^*)(|\mathcal{E}^*| + |V|k^2 + |V|\log|V|))$ since peeling coefficient estimation has complexity $f(k) = O(k^2)$. Specifically, computing the intersection of two KMV sketches has complexity $O(k)$, and k intersections are required since k neighbors are sampled in the KMV sketch. We empirically observed (see Sec. 5.5) that θ^* is small when optimizing triangle-density. Although nodes are removed in ascending order w.r.t. the number of triangles containing them instead of degree, we can still expect a small θ^* in practice since the triangle number is positively correlated with degree.

4.3 Other Density Metrics

In this section, we further briefly describe how to deploy SCANS to other density metrics including p-mean density $\rho_p(S)$ and density metrics with convex/concave size functions $\rho_g(S)$.

p-mean density $\rho_p(S)$ was first proposed by Veldt et al. [40] as a generalization of edge-density.

Definition 9 (p-mean density). *Given a graph $S = (V_S, E_S)$ and parameter $p \in \mathbb{R}$, the p-mean density of S is defined as $\rho_p(S) = (\frac{1}{|V_S|} \sum_{v \in S} N_S(v)^p)^{1/p}$.*

According to the definition of the peeling coefficient in Eq. 1, we can obtain the corresponding peeling coefficient for p-mean density as:

$$\varphi(u) = N(u)^p + \sum_{v \in \mathcal{N}(u)} (N(v)^p - (N(v)-1)^p) \tag{9}$$

Veldt et al. [40] proved that for any $p \geq 1$, the peeling algorithm based on the above peeling coefficient can yield a $(1+p)^{1/p}$-approximation densest subgraph in terms of p-mean density.

To deploy our SCANS system on p-mean density metric, we provide the following estimator for $\varphi_S(u)$ based on KMV sketches by adapting the Horvitz-Thompson estimator:

$$\tilde{\varphi}(u) = \tilde{N}(u)^p + \frac{\tilde{N}(u) \cdot \sum_{v \in \mathcal{K}(u)} (\tilde{N}(v)^p - (\tilde{N}(v)-1)^p)}{k} \tag{10}$$

The estimator for the p-mean density of each subgraph S generated during the peeling iterations can be defined as:

$$\tilde{\rho}_p(S) = (\frac{1}{|V_S|}\sum_{v\in S}\tilde{N}_S(v)^p)^{1/p} \tag{11}$$

List 4 gives the implementation of the SCANS system for p-mean densest subgraph discovery based on the peeling coefficient estimator in Eq. 10 and density estimator in Eq. 11.

```
class PmeanSCANS: public SCANS{
    double coefficient(int v, sketchSet K) {
        double d = val(K[v]), t = 0;
        for(int u: K[v].nbr())
            t += (pow(val(u), p) - pow(val(u)-1, p));
        return pow(d, p) + d * t / K[v].size();
    }
    double density(vector<int> S, sketchSet K){
        double density;
        for(int v: S) density += pow(val(K[v]), p);
        return pow(density / S.size(), 1 / p);
    }
}
```

Listing 4: p-mean densest Subgraph Discovery in SCANS

Density metric $\rho_g(S)$ with general size function $g(S)$. Finally, we discuss how to deploy SCANS system for the optimization of density metrics with general size functions, which generalize the edge-density in another direction.

Definition 10. *Given a subgraph $S = (V_S, E_S)$ and a monotonically non-decreasing function $g : \mathbb{N}^+ \to \mathbb{R}$ with $g(0) = 0$, the size function based density based on g of S is defined as $\rho_g(S) = \frac{|E_S|}{g(|V_S|)}$.*

Kawase and Miyauchi [24] proved that when the function g is either convex or concave, the peeling algorithm with degree as peeling coefficient can be used for $\rho_g(S)$ optimization with certain approximation guarantees. Class `GeneralSizeSCANS` in Listing 5 implements the corresponding peeling algorithm in the SCANS system. The API `coefficient(v, K)` returns the estimated degree of node `v`. For each subgraph `S`, the API `density(S, K)` estimates its density as the summation of the degree of each node in `S` divided by 2 times $g(|V_S|)$.

```
class GeneralSizeSCANS: public SCANS{
    double coefficient(int v, sketchSet K) {
        return val(K[v]);
    }
    double density(vector<int> S, sketchSet K){
        double den;
        for(int v: S) den += coefficient(v, K);
        return den / 2 * g(S.size());
    }
}
```

Listing 5: Densest Subgraph Discovery in SCANS with generalized size function

Table 1: Statistics of KGs used in the experiments, where $|\mathcal{L}(\mathcal{V})|$ and $|\mathcal{L}(\mathcal{E})|$ denote the numbers of node and edge types, and $|\mathbb{M}|$ is the number of evaluated meta-paths.

Dataset	$\lvert\mathcal{V}\rvert$	$\lvert\mathcal{E}\rvert$	$\lvert\mathcal{L}(\mathcal{V})\rvert$	$\lvert\mathcal{L}(\mathcal{E})\rvert$	$\lvert\mathbb{M}\rvert$
IMDB	21.4K	86.6K	4	6	679
ACM	10.9K	548K	4	8	20
DBLP	26.1K	239.6K	4	6	48
PubMed	63.1K	236.5K	4	10	172
FreeBase	180K	1.06M	8	36	151
TPCH	1.85M~29.6M	7.5M~120M	3	2	1

Table 2: Time consumption of relational graph materialization based on boolean matrix multiplication (BoolAP, BoolAP$^+$) and Leapfrog TrieJoin.

Dataset	BoolAP	BoolAP$^+$	Leapfrog TrieJoin
IMDB	0.00017s	0.004s	0.0011s
ACM	19.33s	0.3s	3.0014s
DBLP	4.75s	3.43s	4.7200s
PubMed	15.36s	10.9s	4.4173s
FreeBase	177.04s	110.7s	17.4360s

5 EXPERIMENTS

5.1 Experimental Setup

Datasets. We conduct our experiments on five real-world datasets consisting of KGs and a synthetic dataset corresponding to TPCH, a benchmark relational database. The statistics of the datasets are reported in Table 1. IMDB is a KG about actors and directors of movies. ACM and DBLP are two academic KGs denoting the co-authorships between researchers through papers and publishing venues. PubMed is a biomedical KG representing the relationships between genes, chemicals, and diseases of different species. FreeBase is extracted from a general-purpose KG developed by Google[3]. Furthermore, we make use of the synthetic TPCH dataset [1] with various scale factors for evaluating scalability.[4]

Meta-path Generation. We use AnyBURL [28] to extract a set of candidate meta-paths $\mathbb{M}$. We set the confidence threshold to 0.1 for AnyBURL and take the snapshot at ten seconds. Column $|\mathbb{M}|$ in Table 1 shows the number of meta-paths found on each dataset.

Compared Methods. To our best knowledge, no prior works have focused on DSD over *unmaterialized* relational graphs. We thus compare peeling algorithms implemented through our SCANS framework with algorithms based on explicit relational graph materialization. For fairness of comparison, we wanted to give the baselines the advantage of the most efficient materialization. We experimented with various approaches for relational graph materialization including matrix multiplication [18] and Leapfrog TrieJoin [39]. We found Leapfrog TrieJoin to be the most efficient.[5] Specifically, Table 2 reports the time consumption of methods BoolAP and BoolAP$^+$ [18] based on boolean matrix multiplication as well as Leapfrog TrieJoin for relational graph materialization across datasets. We can observe that over large datasets PubMed and FreeBase, Leapfrog TrieJoin is significantly faster than BoolAP

[3] https://developers.google.com/freebase

[4] Details of our implementation of meta-path evaluation against TPCH are given in the scalability part in Sec. 5.2.

[5] Leapfrog TrieJoin is also known to be worst-case optimal.

and BoolAP$^+$. Thus, we adopt Leapfrog TrieJoin to materialize the relational graph for all baselines.

- FlowE [17] and FlowT [31] apply the max-flow method to find the optimal densest subgraph given the materialized relational graph in terms of edge-density and Δ-density respectively.
- CoreExact [48] is a core-based exact algorithm for DSD in terms of edge-density.
- KCCA [47] is a counting-based approach for exact DSD in terms of Δ-density.
- PeelE [10] and PeelT [38] apply the peeling paradigm to find the approximate densest subgraph given a materialized relational graph, in terms of edge-density and Δ-density respectively.
- ScansE and ScansT are peeling algorithms implemented through SCANS in terms of edge-density and Δ-density respectively.

Fang et al. [13] propose to use edge- and vertex-disjoint core models for community search over meta-path induced relational graphs. While effective for certain meta-paths, this model is not suitable for general meta-paths with extra node constraints due to its rigid topological restriction. For example, in IMDB, it will only return an edge/vertex-disjoint 2-core for 28.7% and 26.8% meta-paths discovered by AnyBURL respectively. Thus, we do not compare with these models.

Parameter Setting. In our experiments, we set $k = 24$, $k^- = 4$ and $\theta = 1$ for both ScansE and ScansT by default. We conduct parameter sensitivity analysis of k and θ for efficiency and effectiveness in Sec. 5.2 and Sec. 5.3 respectively, and choose the default values of hyperparameters to ensure that ScansE and ScansT return a subgraph with a density larger than 0.95 of the densities achieved by methods based on materialized relational graphs on average across datasets, while minimizing the time consumption. Results in Sec. 5.3 demonstrate that peeling algorithms based on our SCANS framework with default parameters can in practice yield results comparable to materialization-based peeling methods .

Evaluation Metrics. (1) For efficiency, we report the average runtime of each algorithm to find the densest subgraph per meta-path. (2) For effectiveness, we quantify by the ratio γ between the density of the subgraph returned by our methods (ScansE and ScansT) and the density achieved by the corresponding materialization-based peeling methods (PeelE and PeelT).

Environment. All experiments are conducted on a Linux Server with AMD EPYC 7643 CPU and 256 GB memory running Ubuntu 20.04. All algorithms are implemented in C++ with -O3 optimization and executed in a single thread.

5.2 Efficiency Evaluation

Time Consumption. In Table 3, we present the execution time per meta-path for each method. We have the following observations.

First, our methods ScansE and ScansT based on the SCANS framework are much more efficient than materialization-based methods. Materialization-based methods cannot handle all experimental cases in reasonable time. FlowE and FlowT can only handle small datasets: FlowE does not terminate in 24 hours except on datasets IMDB and ACM, while FlowT only completes on IMDB, due to time-consuming global flow computations. CoreExact is more efficient than FlowE as it performs flow computation only on dense cores. Nevertheless, it still cannot handle datasets PubMed and FreeBase within 24 hours due to time-consuming flow computations. Materialization-based methods KCCA and PeelT for Δ-density do not complete on DBLP, PubMed, and FreeBase due to the time consuming triangle counting or enumeration operation. In contrast, our methods can handle all experimental cases efficiently. ScansE and ScansT complete on the largest dataset FreeBase within 0.34 and 3.64 seconds per meta-path respectively on average. Compared to materialization-based peeling methods, ScansE achieves up to ∼53× speedup over PeelE on PubMed and FreeBase, and ScansT achieves up to 1063× speedup over PeelT on ACM.

Second, we can observe that methods based on SCANS system are more robust to complex density metrics than prior peeling algorithms based on materialization, in terms of efficiency. To see this, notice that for PeelE optimizing edge-density metric, the relational graph materialization stage dominates its time consumption. The materialization time consistently occupies more than 85% of total time of PeelE across datasets and up to 99.58% on dataset ACM. However, this ratio drops significantly for PeelT optimizing Δ-density, which is much more time-consuming than PeelE. Specifically, on dataset ACM, PeelE finds the densest subgraph based on edge-density within 3.0141 seconds, whereas the corresponding method PeelT requires 743.11 seconds for finding the densest subgraph based on Δ-density on average due to time consuming triangle enumeration. On the other hand, ScansT can still find densest subgraphs based on Δ-density efficiently. The reason is that leveraging the KMV sketches of limited size, ScansT can restrict the time-consuming computations of peeling coefficients and thus the running time becomes less sensitive to the density metrics.

Overall, SCANS accelerates DSD by simultaneously avoiding the high computational overhead of materialization and also expediting the time-consuming peeling coefficient computation.

Memory Usage. Fig. 3 compares the memory usage of the materialized relational graph required by PeelE and PeelT with the KMV sketches utilized by ScansE and ScansT. For each dataset, we report the peak memory usage among all meta-paths. We have the following observations.

First, the additional memory usage required by the KMV sketches is consistently smaller than that of the materialized relational graphs across all datasets. Furthermore, the gap between the memory usage of KMV sketches and materialized relational graphs increases with the increase in the sizes of datasets. Specifically, on small datasets IMDB, KMV sketches requires 7.7× less memory than the the materialized relational graphs, whereas on the large dataset FreeBase, KMV sketches require up to 471× less additional memory than materializing the relational graphs explicitly. The reason is that the memory usage of KMV sketches is linear in the number of nodes in the dataset, whereas the materialized relational graph can consume up to the square of number of nodes in the dataset in the worst case.

Scalability. In this section, we test the scalability of methods based on SCANS through experiments over large synthetic datasets generated by the TPCH benchmark with scale factors $\lambda \in \{1, 2, 4, 8, 16\}$. We conduct our experiments with the meta-path (customer)→(order)→(product), which includes a relational graph connecting pairs of customers who bought the same product [43]. We can observe that both the running time and the memory usage of KMV

Table 3: Results for the efficiency of different algorithms. For algorithms based on materialization, the returning time of each dataset is reported. For ScansE and ScansT, we additionally report the speedup ratios over PeelE and PeelT, and the number of reconstructed sketches θ^*. We also report the time consumption for relational graph materialization in the last column. Cells with a dash line denote that the method cannot be finished within 24 hours.

Metric	ρ_e						ρ_Δ						Materialize
Method	FlowE	CoreExact	PeelE	ScansE			FlowT	KCCA	PeelT	ScansT			
				Time	Speedup	θ^*				Time	Speedup	θ^*	
IMDB	0.0017s	0.0018s	0.0013s	0.0008s	**1.53×** ⇑	1.24	0.1430s	0.0570s	0.0020s	0.0018s	**1.10×** ⇑	1.24	0.0011s
ACM	31.6030s	19.5700s	3.0141s	0.2400s	**12.60×** ⇑	4.75	-	2779.63s	723.11s	0.6800s	**1063×** ⇑	4.65	3.0014s
DBLP	-	624.87s	4.8328s	0.1554s	**31.00×** ⇑	10.02	-	-	-	1.5500s	-	10.48	4.7200s
PubMed	-	-	4.5380s	0.0850s	**53.40×** ⇑	5.22	-	-	-	1.0100s	-	5.20	4.4173s
FreeBase	-	-	18.0464s	0.3400s	**53.10×** ⇑	8.27	-	-	-	3.6400s	-	9.32	17.4360s

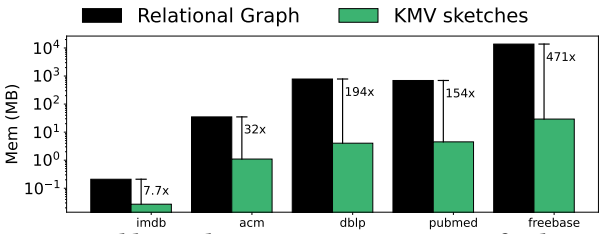

Figure 3: Additional memory consumption of relational graphs materialized in PeelE/PeelT, and KMV sketches constructed in ScansE/ScansT.

sketches are linear in the size of the dataset, which verifies the scalability of SCANS based methods. Specifically, our method ScansE and ScansT can handle the largest TPCH dataset with ~30M nodes within 260 seconds and 436 seconds respectively with 7.72GB additional memory for KMV sketches.

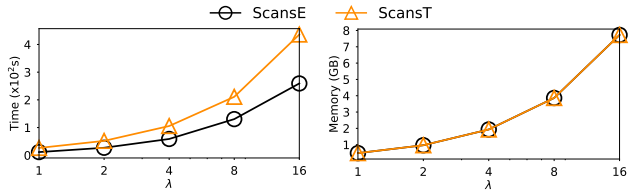

(a) Running Time (b) Memory Usage

Figure 4: The running time and memory usage of methods ScansE and ScansT. The x axis uses a log scale.

Parameter Analysis. We further study the influence of the KMV sketch parameters k and θ over the efficiency of our algorithms. Fig. 6(a)-6(e) reports the running time of ScansE while varying k and θ across datasets. Since the value of k can influence θ^*, the number of KMV sketches that need to be reconstructed, we also track it in Fig. 6(f)-6(j). We can observe that with the increase of k, the running time of ScansE decreases monotonically across all datasets except ACM and PubMed, on which the time of ScansE first decreases when k is varied from 8 to 12 (resp. 16) and then increases (resp. slightly increases) with further increase of k. The reason is that with the increase of k, the number of KMV sketches to be reconstructed θ^* decreases and thus makes the algorithm less time-consuming (confirmed by the trends depicted in Fig. 6(f)–6(j)). However, when the value k reaches a break point (e.g., > 12 on ACM and > 16 on PubMed), the time for KMV sketches construction and peeling coefficient estimation based on KMV sketches becomes the dominant factor and thus the running time starts to increase with

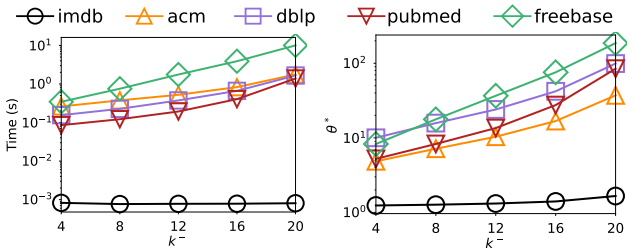

(a) Running Time of ScansE (b) Number of KMV sketches reconstructed θ^* of ScansE

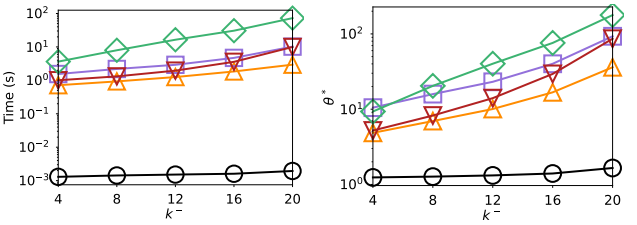

(c) Running time of ScansT (d) Number of KMV sketches reconstructed θ^* of ScansT

Figure 5: Efficiency Analysis of ScansE and ScansT varying parameter k^- across datasets. Subfigure (a) and (b) reports the time consumption and the number of sketches reconstructed θ^* of ScansE; subfigure (c) and (d) reports the corresponding evaluation metrics of ScansT.

k. For the other datasets, it is conceivable that the break point will be reached at larger values of k, i.e., $k > 24$.

On the other hand, with the increase of θ, the running time of ScansE increases significantly. The reason is that the larger value of θ increases the time for KMV sketch construction and peeling coefficient estimation and increases the number of sketches reconstructed θ^* during the peeling iterations.

For ScansT, the value k influences its running time in an opposite direction. Fig. 6(k)– 6(o) reports the running time of ScansT while varying k and θ across datasets. We can observe that with the increase of sketch size k, the running time of ScansT increases monotonically across datasets except FreeBase, even though the number of reconstructed sketches θ^* follows the same distribution as for ScansE (see Fig. 6(p)–6(t)). The reason is that the time needed for peeling coefficient computation for Δ-density metric is influenced by k more significantly. As discussed in Sec. 4.2, the time complexity of method ScansT is $O(k^3)$ due to the estimation of triangles containing each node, compared with $O(k^2)$ for ScansE. Thus, the time consumption for peeling coefficient estimation starts

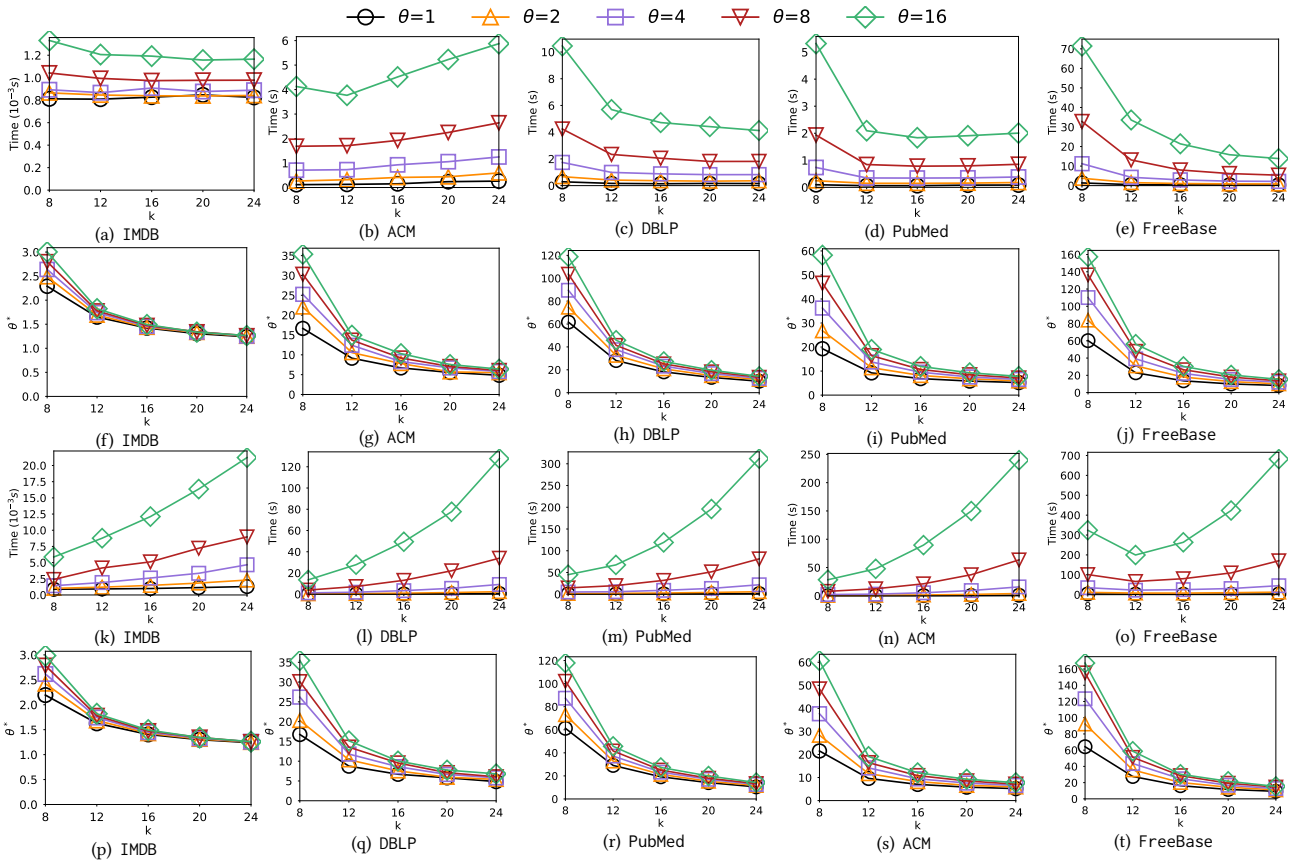

Figure 6: Efficiency analysis of ScansE and ScansT varying k and θ. Subfigures (a)-(e) reports the running time of ScansE; subfigures (f)-(j) reports the number of reconstructed sketches during peeling iterations of ScansE; subfigures (k)-(o) reports the running time of ScansT; subfigures (p)-(t) reports the number of reconstructed sketches during peeling iterations of ScansT.

to dominate the running time of ScansT even for relatively small values of k and it only increases with the increase of k.

Fig. 5 reports the time consumption and the number of KMV sketches reconstructed θ^* of ScansE and ScansT varying parameter k^- across datasets. We can observe that both the time consumption of ScansE and ScansT grows exponentially with the increase of parameter k^- due to the exponential increase of number of sketches reconstructed during the peeling iterations.

5.3 Effective Evaluation

For gauging effectiveness, we compare the density of the subgraph returned by ScansE (resp. ScansT) with that returned by PeelE (resp. PeelT), the materialization based peeling algorithm. Fig. 7 reports the average ratio γ between the edge-density of subgraph returned by ScansE and the edge-density of subgraph returned by PeelE across datasets while varying parameters k and θ.

We first observe that the value γ increases monotonically with both k and θ across all datasets and approaches 1, which is consistent with Theorem 3 that ScansE provides a $(2+\epsilon)$-approximation to the DSD problem based on edge-density ρ_e.

Furthermore, the effectiveness of ScansE is affected by the sketch size k more significantly than by the number of sketches θ. Thus, in order to achieve better effectiveness, users may prefer to increase the sketch size k instead of increasing the number of sketches θ. For example, in FreeBase, increasing k from 8 to 16, fixing $\theta = 1$, boosts γ from 90% to 95%, whereas increasing θ from 4 to 8, fixing $k = 8$, boosts γ from 95% to 97%. Following this observation, we choose the default values of $k = 24$ and $\theta = 1$, which ensures that ScansE achieves $\gamma > 95\%$ across all datasets. For ScansT, we only compare the effectiveness of ScansT with PeelT on IMDB and ACM, the two datasets on which PeelT finishes in reasonable time. We find that ScansT returns subgraphs corresponding to a γ of 99.65% and 95.7% on IMDB and ACM respectively.

Table 4: The ratio between the size of densest subgraph discovered by ScansE and PeelE.

Dataset	IMDB	ACM	DBLP	PubMed	FreeBase
Size ratio	101.6%	102.9%	102.1%	101.9%	102.5%

Table 4 reports the average ratio between the size of densest subgraphs discovered by our method ScansE and the materialization-based peeling method PeelE. We can observe that our method ScansE reveals densest subgraphs with comparable sizes (consistently less than 3% relative differences across datasets) to the densest subgraphs discovered by PeelE.

Overall, by setting the default value of $k = 24$ and $\theta = 1$, both our methods ScansE and ScansT are able to achieve 95%-approximation

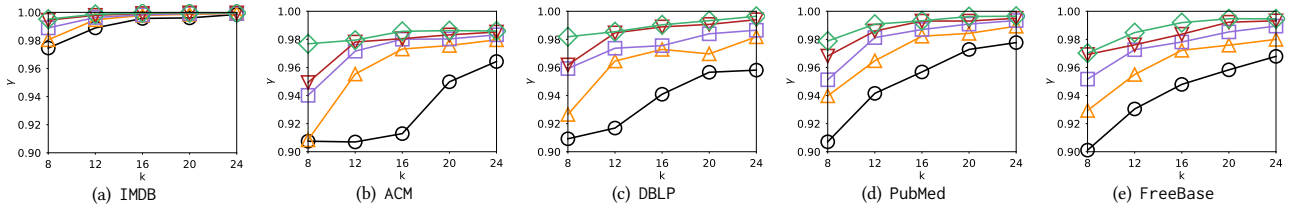

(a) IMDB (b) ACM (c) DBLP (d) PubMed (e) FreeBase

Figure 7: Effectiveness analysis of ScansE with varying parameters k and θ (Share legend with Fig. 6).

to the density of the subgraphs and comparable sizes returned by the corresponding materialization-based peeling methods.

5.4 Case Study

To further gauge the effectiveness of SCANS over real-world applications, we apply ScansE and ScansT on heterogeneous data obtained from our anonymous industrial collaborator, which is one of the leading technology companies known for its diverse services including digital payments and food delivery. We obtain three different types of nodes – *account*(A), *merchant*(M), *device*(D) and two types of edges account→merchant ("order"), account→device ("login"). We choose the meta-path "(account) → (device)" which induces a relational graph connecting two accounts if they login through the same device. Such a relational graph tends to form dense subgraphs containing fraudulent accounts. For each account in the dataset, it contains a ground-truth label denoting whether this account is a fraudster. In scenarios such as artificially inflating a merchant's ranking and visibility through bulk ordering, fraudsters typically create numerous accounts to post positive reviews. These fraudulent actions often lead to the creation of a significant number of accounts, each logging in once, which results in a sparse representation in the heterogeneous graph, making many fraudulent accounts undetectable by DSD applied on the heterogeneous graph directly. However, as long as these accounts are connected through shared devices, they will form dense subgraphs on the relational graph, thus finding the densest subgraph on the relational graph is more promising for finding the fraudulent accounts.

Figure 8 illustrates the fraudulent community identified by our method ScansE (Fig. 8(a)) and a normal community (Fig. 8(b)) formed through device sharing between family members. Traditional DSD methods cannot distinguish the fraudulent community from the normal one within the heterogeneous graph. Specifically, the normal community has density 1.875 in the original heterogeneous data (Fig. 8(b) left), which is even larger than the density of fraudulent community (Fig. 8(a) left). On the other hand, by finding the communities on the relational graphs induced by "(account) → (device)", the density of the fraudulent community (Fig. 8(a) right) increases to 38.05, which is significantly larger than the corresponding density of the normal community (Fig. 8(b) right). Of the 135 accounts flagged by ScansE, 132 are genuinely fraudulent accounts, with 3 being normal accounts (false positives), resulting in a precision of 97.8%. Similarly, the Δ-density-based method, ScansT, identifies the same fraudulent community as ScansE, along with an additional component comprising 9 fraudulent accounts, thus achieving a slightly higher precision of 98.6%.

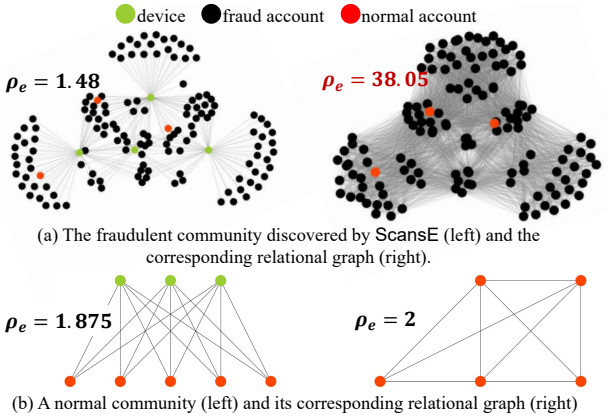

(a) The fraudulent community discovered by ScansE (left) and the corresponding relational graph (right).

(b) A normal community (left) and its corresponding relational graph (right)

Figure 8: Fraudulent community returned by ScansE (Subfigure (a)) and a normal community (Subfigure (b)).

5.5 Synthetic Analysis of θ^*

In addition to reporting the parameter θ^* for the real-world datasets, we explore possible factors that may influence the number of sketch reconstructions θ^* in our SCANS based peeling algorithms. To that end, we perform an analysis of θ^* over synthetic graphs generated with different models. Specifically, we examine the random binomial graphs and the scale-free graphs generated with the Erdős–Rényi (ER) model and Barabási–Albert (BA) model respectively. Fig. 9 reports the value of θ^* while varying the number of nodes $|V|$ in the graph exponentially from 1000 to 16000. The value of θ^* grows logarithmically with the number of nodes $|V|$ in the synthetic graphs on both binomial graphs (Fig. 9(a) and 9(b)) and scale-free graphs (Fig. 9(c) and 9(d)), for both methods ScansE and ScansT. Based on this observation, we conjecture that the number of reconstructed sketches required by the peeling algorithm ScansE and ScansT are logarithmic in the number of nodes in the graph regardless of the specific structure of the relational graphs. We leave a formal proof (or counterexample) of this conjecture as a future work.

6 CONCLUSION

In this paper we introduce SCANS, a materialization-free system for DSD over relational graphs. Our system, grounded in the *sketch-peeling* approach, facilitates efficient estimation of peeling coefficients and subgraph density during peeling iterations directly from heterogeneous data sources. Additionally, we craft user-friendly APIs within the SCANS system, making it simpler for users to implement a variety of peeling algorithms for different density metrics. We establish that SCANS can achieve constant approximation guarantees for DSD based on both edge- and Δ-density. Extensive experiments show that peeling algorithm based on the SCANS system are significantly more efficient than baselines across various

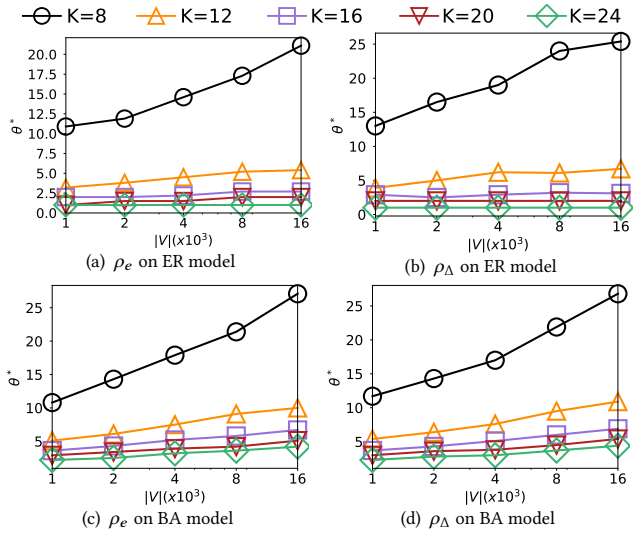

(a) ρ_e on ER model (b) ρ_Δ on ER model

(c) ρ_e on BA model (d) ρ_Δ on BA model

Figure 9: Number of sketches reconstructed θ^* during peeling iteration with varying sizes of synthetic graphs.

datasets based on both edge- and Δ-density, while returning subgraphs whose density is over 95% that of the subgraphs found by traditional materialization-based peeling algorithms.

REFERENCES

[1] [n.d.]. https://www.tpc.org/tpch/.

[2] Daniel J. Abadi, Adam Marcus, Samuel Madden, and Kate Hollenbach. 2009. SW-Store: a vertically partitioned DBMS for Semantic Web data management. *VLDB J.* 18, 2 (2009), 385–406.

[3] Diego Arroyuelo, Aidan Hogan, Gonzalo Navarro, Juan L. Reutter, Javiel Rojas-Ledesma, and Adrián Soto. 2021. Worst-Case Optimal Graph Joins in Almost No Space. In *Proceedings of the 2021 International Conference on Management of Data (SIGMOD '21)*. Association for Computing Machinery, New York, NY, USA, 102–114.

[4] Bahman Bahmani, Ravi Kumar, and Sergei Vassilvitskii. 2012. Densest Subgraph in Streaming and MapReduce. *Proc. VLDB Endow.* 5, 5 (2012), 454–465.

[5] Ziv Bar-Yossef, TS Jayram, Ravi Kumar, D Sivakumar, and Luca Trevisan. 2002. Counting distinct elements in a data stream. In *Randomization and Approximation Techniques in Computer Science: 6th International Workshop, RANDOM 2002 Cambridge, MA, USA, September 13–15, 2002 Proceedings 5*. Springer, 1–10.

[6] Kevin S. Beyer, Peter J. Haas, Berthold Reinwald, Yannis Sismanis, and Rainer Gemulla. 2007. On Synopses for Distinct-Value Estimation under Multiset Operations. In *Proceedings of the 2007 ACM SIGMOD International Conference on Management of Data (SIGMOD '07)*. Association for Computing Machinery, New York, NY, USA, 199–210.

[7] Francesco Bonchi, Arijit Khan, and Lorenzo Severini. 2019. Distance-generalized Core Decomposition. In *Proceedings of the 2019 International Conference on Management of Data, SIGMOD Conference 2019, Amsterdam, The Netherlands, June 30 - July 5, 2019*. ACM, 1006–1023.

[8] Digvijay Boob, Yu Gao, Richard Peng, Saurabh Sawlani, Charalampos E. Tsourakakis, Di Wang, and Junxing Wang. 2020. Flowless: Extracting Densest Subgraphs Without Flow Computations. In *WWW '20: The Web Conference 2020, Taipei, Taiwan, April 20-24, 2020*. ACM / IW3C2, 573–583.

[9] Bokai Cao, Mia Mao, Siim Viidu, and Philip S. Yu. 2017. HitFraud: A Broad Learning Approach for Collective Fraud Detection in Heterogeneous Information Networks. In *2017 IEEE International Conference on Data Mining, ICDM 2017, New Orleans, LA, USA, November 18-21, 2017*. IEEE Computer Society, 769–774.

[10] Moses Charikar. 2000. Greedy approximation algorithms for finding dense components in a graph. In *Approximation Algorithms for Combinatorial Optimization, Third International Workshop, APPROX 2000, Saarbrücken, Germany, September 5-8, 2000, Proceedings (Lecture Notes in Computer Science)*, Vol. 1913. Springer, 84–95.

[11] Serafeim Chatzopoulos, Thanasis Vergoulis, Dimitrios Skoutas, Theodore Dalamagas, Christos Tryfonopoulos, and Panagiotis Karras. 2023. Atrapos: Real-time Evaluation of Metapath Query Workloads. In *Proceedings of the ACM Web Conference 2023 (WWW '23)*. Association for Computing Machinery, New York, NY, USA, 2487–2498.

[12] Edith Cohen, Eran Halperin, Haim Kaplan, and Uri Zwick. 2002. Reachability and distance queries via 2-hop labels. In *Proceedings of the Thirteenth Annual ACM-SIAM Symposium on Discrete Algorithms, January 6-8, 2002, San Francisco, CA, USA*. ACM/SIAM, 937–946.

[13] Yixiang Fang, Yixing Yang, Wenjie Zhang, Xuemin Lin, and Xin Cao. 2020. Effective and Efficient Community Search over Large Heterogeneous Information Networks. *Proc. VLDB Endow.* 13, 6 (2020), 854–867.

[14] Yixiang Fang, Kaiqiang Yu, Reynold Cheng, Laks VS Lakshmanan, and Xuemin Lin. 2019. Efficient algorithms for densest subgraph discovery. *Proceedings of the VLDB Endowment* 12, 11 (2019), 1719–1732.

[15] Michael J. Freitag, Maximilian Bandle, Tobias Schmidt, Alfons Kemper, and Thomas Neumann. 2020. Adopting Worst-Case Optimal Joins in Relational Database Systems. *Proc. VLDB Endow.* 13, 11 (2020), 1891–1904.

[16] Aristides Gionis, Flavio Junqueira, Vincent Leroy, Marco Serafini, and Ingmar Weber. 2013. Piggybacking on Social Networks. *Proc. VLDB Endow.* 6, 6 (2013), 409–420.

[17] A. V. Goldberg. 1984. *Finding a Maximum Density Subgraph.* Technical Report. USA.

[18] Yucan Guo, Chenhao Ma, and Yixiang Fang. 2024. Efficient Core Decomposition over Large Heterogeneous Information Networks. In *40th IEEE International Conference on Data Engineering (ICDE)*. IEEE, to appear.

[19] Aidan Hogan, Eva Blomqvist, Michael Cochez, Claudia d'Amato, Gerard de Melo, Claudio Gutierrez, Sabrina Kirrane, José Emilio Labra Gayo, Roberto Navigli, Sebastian Neumaier, Axel-Cyrille Ngonga Ngomo, Axel Polleres, Sabbir M. Rashid, Anisa Rula, Lukas Schmelzeisen, Juan F. Sequeda, Steffen Staab, and Antoine Zimmermann. 2022. Knowledge Graphs. *ACM Comput. Surv.* 54, 4 (2022), 71:1–71:37.

[20] Daniel G Horvitz and Donovan J Thompson. 1952. A generalization of sampling without replacement from a finite universe. *Journal of the American statistical Association* 47, 260 (1952), 663–685.

[21] Shaoxiong Ji, Shirui Pan, Erik Cambria, Pekka Marttinen, and Philip S. Yu. 2022. A Survey on Knowledge Graphs: Representation, Acquisition, and Applications. *IEEE Trans. Neural Networks Learn. Syst.* 33, 2 (2022), 494–514.

[22] Jiaxin Jiang, Yuhang Chen, Bingsheng He, Min Chen, and Jia Chen. 2024. Spade+: A Generic Real-Time Fraud Detection Framework on Dynamic Graphs. *IEEE Transactions on Knowledge and Data Engineering* (2024).

[23] Yangqin Jiang, Yixiang Fang, Chenhao Ma, Xin Cao, and Chunshan Li. 2022. Effective Community Search over Large Star-Schema Heterogeneous Information Networks. *Proc. VLDB Endow.* 15, 11 (2022), 2307–2320.

[24] Yasushi Kawase and Atsushi Miyauchi. 2018. The Densest Subgraph Problem with a Convex/Concave Size Function. *Algorithmica* 80, 12 (2018), 3461–3480.

[25] Jonathan Kuck, Honglei Zhuang, Xifeng Yan, Hasan Cam, and Jiawei Han. 2015. Query-based outlier detection in heterogeneous information networks. In *Advances in database technology: proceedings. International Conference on Extending Database Technology*, Vol. 2015. NIH Public Access, 325.

[26] Laks V. S. Lakshmanan. 2022. On a Quest for Combating Filter Bubbles and Misinformation. In *SIGMOD '22: International Conference on Management of Data, Philadelphia, PA, USA, June 12 - 17, 2022*. ACM, 2.

[27] Tommaso Lanciano, Atsushi Miyauchi, Adriano Fazzone, and Francesco Bonchi. 2023. A Survey on the Densest Subgraph Problem and its Variants. *arXiv preprint arXiv:2303.14467* (2023).

[28] Christian Meilicke, Melisachew Wudage Chekol, Daniel Ruffinelli, and Heiner Stuckenschmidt. 2019. Anytime Bottom-Up Rule Learning for Knowledge Graph Completion. In *Proceedings of the Twenty-Eighth International Joint Conference on Artificial Intelligence, IJCAI-19*. International Joint Conferences on Artificial Intelligence Organization, 3137–3143.

[29] Shahan Ali Memon and Kathleen M Carley. 2020. Characterizing covid-19 misinformation communities using a novel twitter dataset. *arXiv preprint arXiv:2008.00791* (2020).

[30] Changping Meng, Reynold Cheng, Silviu Maniu, Pierre Senellart, and Wangda Zhang. 2015. Discovering meta-paths in large heterogeneous information networks. In *Proceedings of the 24th international conference on world wide web*. 754–764.

[31] Michael Mitzenmacher, Jakub Pachocki, Richard Peng, Charalampos Tsourakakis, and Shen Chen Xu. 2015. Scalable large near-clique detection in large-scale networks via sampling. In *Proceedings of the 21th ACM SIGKDD International Conference on Knowledge Discovery and Data Mining*. 815–824.

[32] Hung Q. Ngo, Ely Porat, Christopher Ré, and Atri Rudra. 2018. Worst-case Optimal Join Algorithms. *J. ACM* 65, 3, Article 16 (2018), 40 pages.

[33] Chuan Shi, Zhiqiang Zhang, Ping Luo, Philip S Yu, Yading Yue, and Bin Wu. 2015. Semantic path based personalized recommendation on weighted heterogeneous information networks. In *Proceedings of the 24th ACM international on conference on information and knowledge management*. 453–462.

[34] Sriganesh Srihari and Hon Wai Leong. 2013. A Survey of Computational Methods for protein Complex Prediction from protein Interaction Networks. *J. Bioinform. Comput. Biol.* 11, 2 (2013).

[35] Panagiotis Strouthopoulos and Apostolos N Papadopoulos. 2019. Core discovery in hidden networks. *Data & Knowledge Engineering* 120 (2019), 45–59.

[36] Wen Sun, Achille Fokoue, Kavitha Srinivas, Anastasios Kementsietsidis, Gang Hu, and Guo Tong Xie. 2015. SQLGraph: An Efficient Relational-Based Property Graph Store. In *Proceedings of the 2015 ACM SIGMOD International Conference on Management of Data, Melbourne, Victoria, Australia, May 31 - June 4, 2015*, Timos K. Sellis, Susan B. Davidson, and Zachary G. Ives (Eds.). ACM, 1887–1901.

[37] Yizhou Sun, Jiawei Han, Xifeng Yan, Philip S. Yu, and Tianyi Wu. 2011. PathSim: Meta Path-Based Top-K Similarity Search in Heterogeneous Information Networks. *Proc. VLDB Endow.* 4, 11 (2011), 992–1003.

[38] Charalampos E. Tsourakakis. 2015. The K-clique Densest Subgraph Problem. In *Proceedings of the 24th International Conference on World Wide Web, WWW 2015, Florence, Italy, May 18-22, 2015*, Aldo Gangemi, Stefano Leonardi, and Alessandro Panconesi (Eds.). ACM, 1122–1132.

[39] Todd L. Veldhuizen. 2014. Triejoin: A Simple, Worst-Case Optimal Join Algorithm. In *Proceedings of the 17th International Conference on Database Theory (ICDT)*. OpenProceedings.org, 96–106.

[40] Nate Veldt, Austin R. Benson, and Jon M. Kleinberg. 2021. The Generalized Mean Densest Subgraph Problem. In *KDD '21: The 27th ACM SIGKDD Conference on Knowledge Discovery and Data Mining, Virtual Event, Singapore, August 14-18, 2021*. ACM, 1604–1614.

[41] Bryan Wilder, Nicole Immorlica, Eric Rice, and Milind Tambe. 2018. Maximizing Influence in an Unknown Social Network. In *Proceedings of the Thirty-Second AAAI Conference on Artificial Intelligence, (AAAI-18), the 30th innovative Applications of Artificial Intelligence (IAAI-18), and the 8th AAAI Symposium on Educational Advances in Artificial Intelligence (EAAI-18), New Orleans, Louisiana, USA, February 2-7, 2018*. AAAI Press, 4743–4750.

[42] Min Wu, Xiaoli Li, Chee Keong Kwoh, and See-Kiong Ng. 2009. A core-attachment based method to detect protein complexes in PPI networks. *BMC Bioinform.* 10 (2009).

[43] Konstantinos Xirogiannopoulos and Amol Deshpande. 2017. Extracting and Analyzing Hidden Graphs from Relational Databases. In *Proceedings of the 2017 ACM International Conference on Management of Data (SIGMOD '17)*. Association for Computing Machinery, New York, NY, USA, 897–912.

[44] Yixing Yang, Yixiang Fang, Xuemin Lin, and Wenjie Zhang. 2020. Effective and Efficient Truss Computation over Large Heterogeneous Information Networks. In *36th IEEE International Conference on Data Engineering (ICDE)*. IEEE, 901–912.

[45] Niu Yudong, Yuchen Li, Ju Fan, and Zhifeng Bao. 2022. Local Clustering over Labeled Graphs: An Index-Free Approach. In *2022 IEEE 38th International Conference on Data Engineering (ICDE)*. IEEE, 2805–2817.

[46] Yingli Zhou, Yixiang Fang, Wensheng Luo, and Yunming Ye. 2023. Influential Community Search over Large Heterogeneous Information Networks. *Proceedings of the VLDB Endowment* 16, 8 (2023), 2047–2060.

[47] Yingli Zhou, Qingshuo Guo, Yixiang Fang, and Chenhao Ma. 2024. A Counting-based Approach for Efficient k-Clique Densest Subgraph Discovery. *Proceedings of the ACM on Management of Data* 2, 3 (2024), 1–27.

[48] Yingli Zhou, Qingshuo Guo, Yi Yang, Yixiang Fang, Chenhao Ma, and Laks Lakshmanan. 2024. In-depth Analysis of Densest Subgraph Discovery in a Unified Framework. *arXiv preprint arXiv:2406.04738* (2024).